Chapter 7
Modeling of Semisolid Processing

7.1 Introductory Remarks on Modeling

Computational fluid dynamics (CFD) can be used to predict die filling. However, input parameters must be obtained from rheological experiments (see Chap. 6. In some cases, the data that has been used is from steady state experiments, where the material has been maintained at a particular shear rate for some time. In cases where the process involves taking material from rest into the die in a fraction of a second, it is difficult to see how this can be appropriate. The material changes viscosity by several orders of magnitude in that fraction of a second [23, 32]. Observations of transient rheological behavior under rapid changes in shear rate are therefore more relevant for input data for modeling.

Modeling of semisolid processing is generally continuum modeling, where the macroscopic behavior is predicted with the internal structure represented by a few internal variables. Continuum modeling for semisolid can be categorized into one-phase or two-phase and as finite difference or finite element. In one-phase modeling, a single non-Newtonian equation of state for the viscosity takes into account the interrelationship between the liquid and the solid through the way in which they behave when they are in combination. In two-phase modeling, each individual phase (the liquid matrix or the solid particles) is characterized with separate equations. The two-phase approach is more complicated, requires significantly higher computational time and much higher effort on obtaining the experimental parameters for input. It is, however, more physically realistic and does allow for important (and undesirable) phenomena, such as liquid segregation to be modeled. Liquid segregation is where liquid gathers in one part of the component in preference to another during processing. Figure 7.1 shows a classic but extreme example. The material is being forced vertically upwards into a die and has to flow around a corner to reach the end of the die. The sharp corner (the dotted line in the inset shows the die shape) causes the liquid to separate from the solid and to gather in one place. In the micrograph, the quenched liquid is dark gray in comparison with the solid. The die has not filled properly. Liquid segregation is deleterious, leading, for example, to inhomogeneous mechanical properties after solidification.

David H. Kirkwood et al., *Semi-solid Processing of Alloys*,
Springer Series in Materials Science,
DOI 10.1007/978-3-642-00706-4_7,

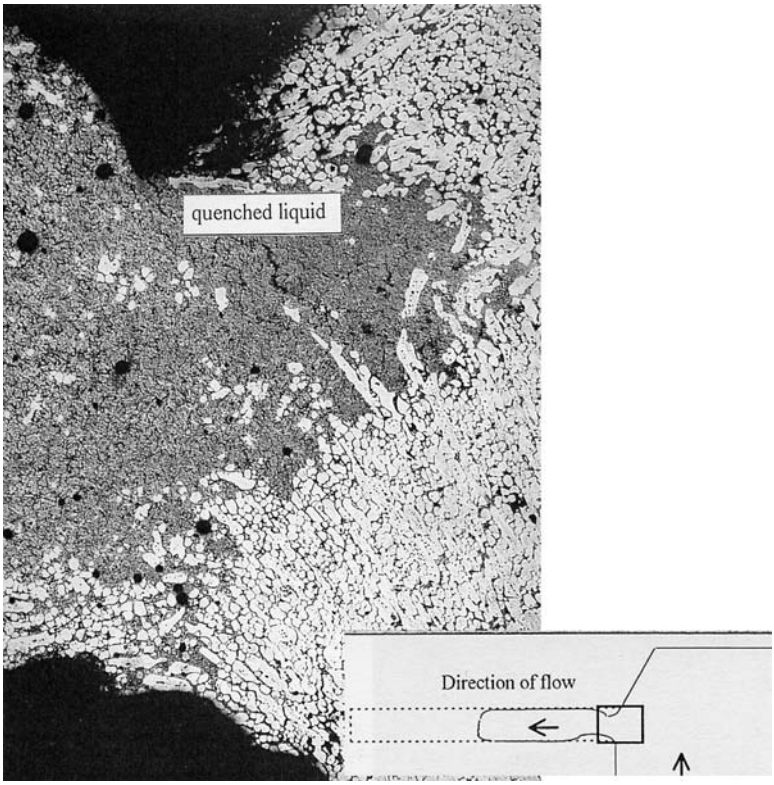

Fig. 7.1 Aluminum alloy 7075 is being forced vertically upwards into a die (*see inset*). The material has to flow around a corner and liquid segregation is occurring at that corner [53], partly because the temperature conditions are inappropriate. The *rectangular outlined portion* is the area shown in the micrograph

Continuum modeling generally requires discretization for analysis. The major methods used in semisolid modeling are the finite difference method and the finite element method. In the finite difference method, approximations for the derivatives at a grid point are chosen. In contrast, in the finite element method, weighting functions are used for the grid nodes. A detailed discussion of these discretization methods is given in [54, 55].

Modeling of semisolid processing, by its very nature, sits at the interface between fluids modeling and solids modeling. The CFD approaches originate in fluids modeling but in semisolid processing must bring in the thixotropic behavior. For higher solid fractions, solid mechanics approaches may be more appropriate. In effect, if fractions of solid are nearer 0.8 or 0.9, the process may be more akin to soft forging. Processing in this regime may not be what we might think of as classical thixo- or rheo-forming. Examining the microstructure after forming will tend to reveal deformed solid spheroids (see Fig. 7.2) rather than the round spheroids, which would

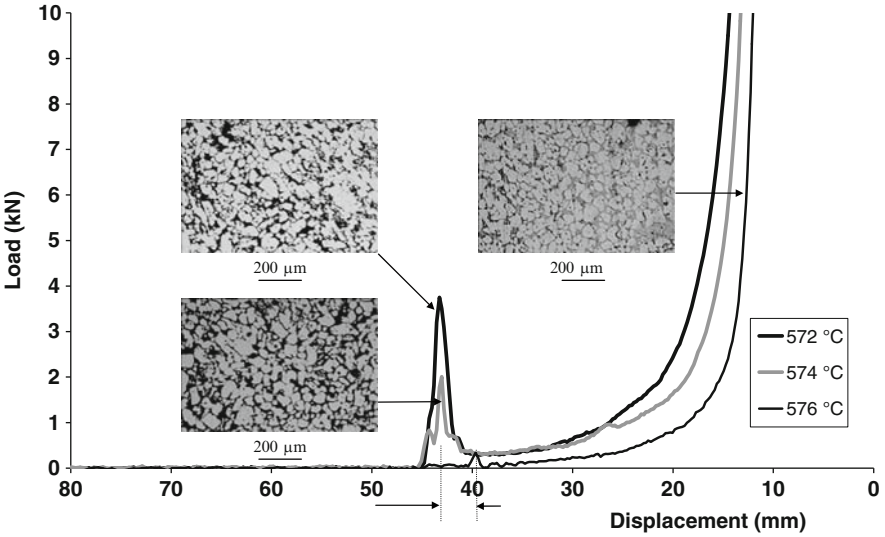

Fig. 7.2 Load versus displacement for the rapid compression of a billet of A357 aluminum alloy in a thixoformer [56], illustrating that at relatively high fraction solid (572°C), the spheroids in the microstructure are deformed. At relatively low fraction solid (576°C), the spheroids are undeformed and the resistance to deformation is low. The closeness of these temperatures shows how sensitive the process is to temperature. The microstructures are taken from the edge of the billet after compression has been completed

be expected to exist throughout the solidified component in classical thixoforming. It is helpful to include consideration of such solid approaches here. In addition, there have been recent developments of micromechanical continuum models (termed here "micromodeling"), which involve the concept of a "coated inclusion" and sit at the interface between fluids modeling and solids modeling.

Previous reviews can be found in [57–60]. Atkinson [59] provides an extensive survey of modeling work in the literature and the validation of the results, including summarizing the approaches taken by different modelers. For details of the mathematical basis, it will be helpful to consult [60]. Here, we take an overview with relatively little mathematical detail. Section 7.2 will highlight the utility of modeling, Sect. 7.3 will introduce the use of the structural parameter λ for modeling and outline the model of Brown and coworkers, which is extensively drawn on by other researchers. Section 7.4 briefly highlights the issue about the use of yield points in modeling. Section 7.5 then covers finite difference modeling and Sect. 7.6 finite element, with one- and two-phase modeling covered in both cases. Models akin to forging models, essentially those where the time dependence of viscosity is not treated, are covered in Sect. 7.7. Micromodeling is then discussed in Sect. 7.8. Some concluding remarks are then given.

7.2 Utility of Modeling

Die design rules from die casting are not transferable to thixoforming and related processes. Figure 7.3 illustrates this problem with a generic demonstrator consisting of a round plate with three bolt holes and a central boss [61]. When preliminary trials were carried out, there was difficulty in filling the die. Partial filling experiments were carried out, which showed that the design of the die, particularly the in-gate, which was narrow and "inward directed" as for die-casting, was leading to some jet flow across the cavity (Fig. 7.3a); i.e., the material was jetting to the end of the cavity and then flowing back on itself. Defects were occurring behind the central boss and on either side just after the entrance. The flow was contrary to the smooth progressive filling, which is the aim in thixoforming.

FLOW3D, which is a CFD program from FLOWSCIENCE Inc., was used to model the flow in the die (Fig. 7.3b), trying out different viscosities in order to find the range in which the experimental behavior was mimicked. The work did not take into account either heat transfer in the die or friction at the die surface. Even so reasonable agreement was found. In addition, the model, in the version used, did not allow for thixotropic behavior as such (i.e., it assumed the fluid had a constant viscosity independent of the shear rate and time, which in practice is not the case). The design of the die was changed as a result of this "simple" modeling and this led to improved filling (Fig. 7.3c). The in-gate was widened and deepened which reduced jet flow. In addition, the bolt holes were made ellipsoidal, which reduced disruption

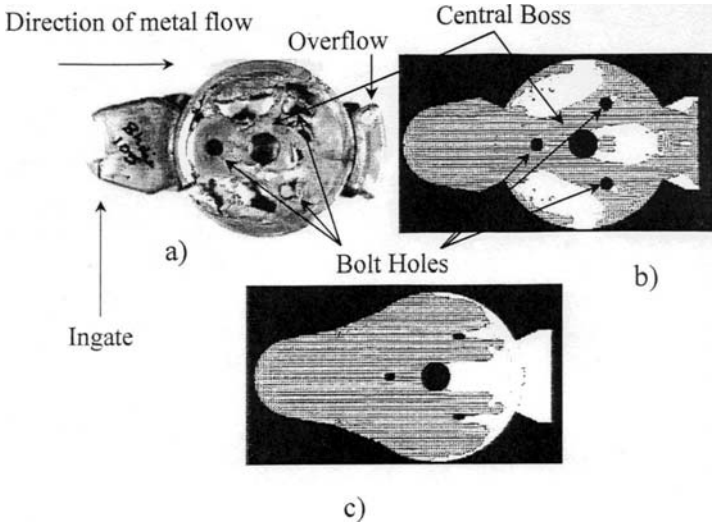

Fig. 7.3 Numerical simulation of die filling [61]. (**a**) Partial filling of die. (**b**) Modeling simulation of (**a**) where *white* corresponds to *dark* on (**a**). (**c**) Modeling simulation with improved die design showing smoother filling

to the flow path. In practice, the latter would not be possible because the shape is dictated by the requirements of the component. However, the wide, deep, smoothly contoured character of the in-gate is now widely recognized to be a requirement for thixoforming. This example illustrates the real potential commercial benefit, which can be obtained from better understanding of flow of semisolid material in dies. The use of modeling can reduce the need for extensive trials of die design, ram speed, dwell time, and pressure.

7.3 Use of the Structural Parameter λ for Modeling: Model of Brown and Coworkers

As described earlier, thixotropy is associated with the formation of bonds between spheroids (and agglomerates of spheroids), when the material is at rest or being sheared at low shear rate. When the shear rate is suddenly increased, some of these bonds will be broken and the viscosity decreases. The extent to which a continuous structure of bonded spheroids is in existence is represented by what is called the structural parameter λ (sometimes called the "single internal variable" in the modeling of semisolid processing). A fully built-up structure is usually represented by $\lambda = 1$ and a completely broken-down structure, with all the spheroids separate from each other, by $\lambda = 0$ [62]. At a particular shear rate, after enough time has elapsed, the processes of break-down and build-up will be in dynamic equilibrium so that a particular value of λ is characteristic of that shear rate. Thixotropy is then introduced mathematically via the time derivative of the structural parameter $\mathrm{d}\lambda/\mathrm{d}t$. This is the balance of the build-up and break-down terms. In the simplest theories, these are only controlled by the shear rate and the current level of the structure parameter λ. The driving force for build-up is controlled by the difference of the structure from its maximum value, i.e., $(1 - \lambda)$, raised to a power b. The rate of break-down due to shearing can be given by the product of the current level of the structure λ and the shear rate $\dot{\gamma}$ raised to another power d. So,

$$\frac{\mathrm{d}\lambda}{\mathrm{d}t} = a\,(1-\lambda)^b - c\lambda\dot{\gamma}^d, \tag{7.1}$$

where a and c are constants for any one system. The system is breaking down towards equilibrium if the overall value of $\mathrm{d}\lambda/\mathrm{d}t$ is negative and building up if it is positive. The Moore model [63] is a simplified version of (7.1) with b and d set to 1. Cheng and Evans [64] set b to 1 but allowed d to take different constant values.

The next step in any model is to relate the structure λ to the stress τ or viscosity η in a flow equation. This has been done in a variety of ways including the simple Bingham model

$$\tau = \tau_\mathrm{y} + k\dot{\gamma}, \tag{7.2}$$

where τ_y is a yield stress, and the Herschel–Bulkley model where the behavior is nonlinear after yield

$$\tau = \tau_y + k\dot{\gamma}^n. \tag{7.3}$$

Brown and coworkers [21,65,66] presented a constitutive model based on the single internal variable concept. The two key equations are

$$\tau = A(\lambda)\frac{(c/c_{max})^{1/3}}{1-(c/c_{max})^{1/3}}\eta_f\dot{\gamma} + (n+1)\,C(T)\,\lambda f_s \eta_f^{n+1}\dot{\gamma}^n, \tag{7.4}$$

$$\frac{d\lambda}{dt} = H(T, f_s)(1-\lambda) - G(T, f_s)\,\lambda\dot{\gamma}^n. \tag{7.5}$$

In (7.4), $A(\lambda)$ is a hydrodynamic coefficient, which is a function of λ, c is the effective volume packing fraction solid and c_{max} the maximum value of that, η_f is the viscosity of the fluid, n is the shear rate exponent, $C(T)$ an exponential function of temperature and f_s the fraction of solid, which is also temperature dependent. In (7.5), H is the agglomeration function and G is the disagglomeration function, both of which are dependent on the temperature and the fraction solid. Brown et al. assume that flow resistance is due to hydrodynamic flow of agglomerates (the first term on the right in (7.4)) and deformation of solid particles within the agglomerates (the second term on the right). The hydrodynamic coefficient $A(\lambda)$ depends on the size, distribution, and morphology of the particle agglomerates. The deformation resistance term arises because of the energy dissipated in the plastically deforming particle–particle bonds. Overall, the model of Brown et al. predicts an increase in the deformation resistance with the solid fraction and this becomes rapid between 0.5 and 0.6 f_s. It is not valid beyond about $0.6 f_s$.

The constitutive equations due to Brown et al. [21, 65, 66] have been used by a number of workers both for finite difference modeling and finite element [67–70], sometimes with the introduction of a yield stress into (7.4) [67].

7.4 Use of a Yield Stress in Models

There are very mixed views about whether a yield point should be used in modeling semisolid processing. A number of the models described below include a yield stress (e.g., those based on Bingham or Herschel–Bulkley equations – see (7.2) and (7.3)). Kirkwood and Ward argue against the use of a yield point [52] (see Sect. 6.4), defining a yield point as the stress approached, as the flow is reduced. This is distinct from the peak seen in compression tests, which is associated with the initial structural breakdown of the solid "skeleton." This is of a different magnitude from that proposed in Bingham or Herschel–Bulkley modeling.

7.5 Finite Difference Modeling

7.5.1 One-phase Finite Difference Modeling

Ilegbusi and Brown [67] used the Brown et al. model (see Sect. 7.3) with a yield stress to examine flow into a chisel-shaped cavity. A solid shell formed at the mould wall leading to "jetting" in the center of the cavity and hence showing the importance of heating the die and the heat transfer coefficient.

A commercial code called FLOW3D has had a thixotropic module incorporated. The mathematical approach is outlined in [71, 72]. The two key equations are given as (7.6) and (7.7). A transport equation (7.6) is used for the viscosity η rather than for the structural parameter λ (as in the Brown et al. model), because this is convenient for computational fluid dynamics, which requires a value for η.

$$\frac{\partial \eta}{\partial t} + \underline{u} \cdot \nabla \eta = \omega \left(\eta_e - \eta \right), \tag{7.6}$$

$$\frac{\partial \lambda}{\partial t} + \underline{u} \cdot \nabla \lambda = b_1 \left(1 - \lambda \right) + b_2 \lambda \dot{\gamma}. \tag{7.7}$$

$\underline{u}$ is the velocity vector, ω is the inverse of the relaxation time, η_e is the steady state equilibrium viscosity and b_1, b_2 are constants. The second term on the left of (7.6) is the advection term and the term on the right is the relaxation term. The relaxation depends on the steady state viscosity η_e and the relaxation time $1/\omega$. Both of these variables depend on shear rate and solid fraction. The model does not include yield stress, wall slip, or elastic or plastic behavior at high solid fractions. It is most relevant where fractions solid are less than about 0.7. Agglomeration and disagglomeration are represented on the right hand side in (7.7). Here disagglomeration is dependent on $\dot{\gamma}$, and not $\dot{\gamma}^n$ as in (7.5) in the model of Brown and his coworkers. The model has been used to predict hysteresis curves for semisolid Sn15%Pb with a reasonable degree of accuracy [71]. Equations (7.6) and (7.7) are in fact equivalent, but both are given here for clarity in explanation.

The rate coefficient ω used by Barkhudarov et al. [72] has a linear dependence on shear rate $\dot{\gamma}$. This can be compared with that of Kirkwood and Ward [52], which has a linear dependence on $\dot{\gamma}^m$. If $m = 1$, the two equations for ω are equivalent.

Barkudarov et al. present their model in slightly different terms [72], which is helpful for developing understanding. They used equation

$$\frac{\partial \eta}{\partial t} + \underline{u} \cdot \nabla \eta = \alpha \mathrm{Min} \left(\eta_e - \eta, 0 \right) + \beta \mathrm{Max} \left(\eta_e - \eta, 0 \right). \tag{7.8}$$

$\mathrm{Min}\left(\eta_e - \eta, 0\right)$ means take the lower value of $\eta_e - \eta$ and 0 and $\mathrm{Max}\left(\eta_e - \eta, 0\right)$ means take the higher of the two values. If $\eta_e - \eta < 0$, then the right hand side is equal to $\alpha \left(\eta_e - \eta\right)$ and if $\eta_e - \eta > 0$, then the right hand side is equal to $\beta \left(\eta_e - \eta\right)$. What this means is that if the local viscosity is greater than the equilibrium viscosity η_e, then the local viscosity is driven towards η_e at the thinning rate α. If

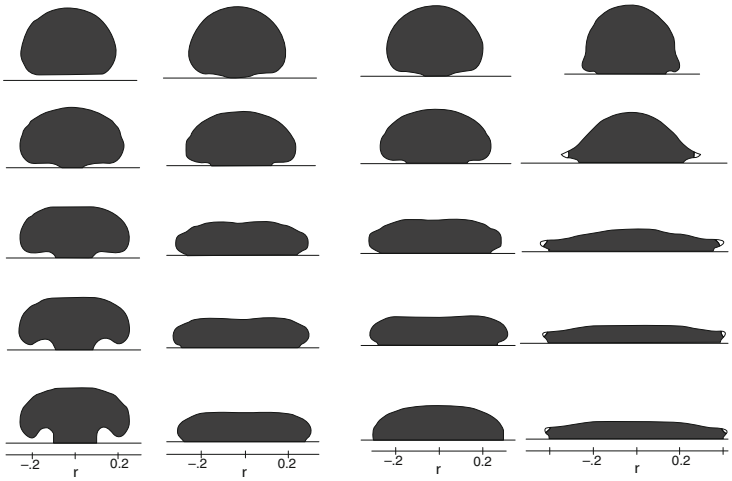

Fig. 7.4 Comparison of the effect of thixotropic relaxation time when a droplet of Sn15wt%Pb is allowed to fall from rest onto a plate located 6 cm below [72]. The droplet is assumed to be at 197°C with approximately 47% solid fraction. Heat transfer to the plate is taken into account. Relaxation times (in ms) from *top to bottom* are 1, 2, 5, 10, and 50. The *first column on the left* has a zero rate, i.e., constant viscosity. The *second* has thinning and thickening rates of $1{,}000\,s^{-1}$. The *third column* has a $1{,}000\,s^{-1}$ thinning rate and a 0.0001 thickening rate. The *last column* has infinitely fast rates

the local viscosity is less than the equilibrium viscosity η_e, then the local viscosity is driven towards η_e at the thickening rate β. α and β will be dependent on the shear rate and it is known that shear thinning tends to be much faster than shear thickening. Figure 7.4 [72] shows the results for a droplet of Sn15wt%Pb impacting on a flat plate having been dropped from rest 6 cm above it. The columns show the behavior for different relaxation times. Infinitely fast relaxation gives very fast "spreading" (see the extreme right hand column in the Fig. 7.4). Zero relaxation leads to a mushroom-type shape (see the extreme left hand column in the figure). Figure 7.5 [72] shows detail of the impact process with surface tension dominating initially, but then gravity taking over in governing the behavior.

A number of workers have used the FLOW3D thixotropic module [73–77] for modeling semisolid processing. Modigell and Koke [73] used the Herschel–Bulkley model (7.3) with the yield stress τ_y dependent on the fraction of solid. They modified the nature of the structural parameter making it into one, which varies between 0 for fully broken-down and infinity for fully built-up (rather than between 0 and 1). The time evolution of the structural parameter is described with first-order reaction kinetics. The model fits shear rate experiments with Sn15%Pb, where the shear rate undergoes step changes, quite well. The parameters are obtained by iterative adjustment. Figure 7.6 shows simulation of die fill in a cavity with a cylindrical obstacle, contrasting the behavior with Newtonian and thixotropic fluids. With Newtonian fluid, the flow jets past the obstacle and hits the end of the cavity before beginning to flow back on itself. The thixotropic fluid is flowing smoothly past the obstacle

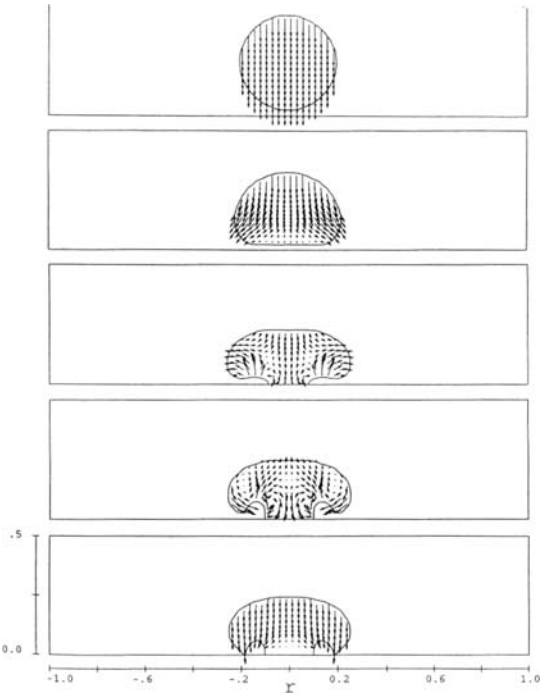

Fig. 7.5 Impact of a viscous drop with the same material as for Fig. 6.5 [72]. Times in ms from *top to bottom* are 0, 1, 5, 50, 100. Surface tension is dominating the flow in the 5–50 ms period; gravity is dominant by 100 ms

and the flow front may well meet and remerge with the material flowing on the left hand side of the obstacle (but not shown here because of symmetry).

Modigell and Koke [51] found that above a critical inlet velocity the filling was not laminar any more. They found that they could represent the transition between laminar and turbulent filling (in the sense of a smooth flow front and one that is starting to break up) reasonably well.

The FLOW3D thixotropic module can be used to model rheometry experiments (with a concentric cylinder viscometer, for example) as well as die fill. It is important to ensure that possible sources of error in modeled shear stress curves for rheometry experiments are understood. When the inner cylinder of a viscometer (the "bob") is accelerated, a finite time is required for the momentum to propagate across the gap between the cylinders. This diffusion produces a stress peak, even in Newtonian fluids. The propagation time (which is equivalent to the width of the shear stress peak) can be calculated approximately, based on the momentum diffusion equation in a plane sheet [74],

$$t = 0.45\frac{x^2}{\nu}, \tag{7.9}$$

where x is the gap width between the rotating cylinder and the cup and ν is the kinematic viscosity, i.e., η/ρ, where η is the fluid viscosity and ρ the density. For a fluid of 1 Pa.s viscosity, the time is $\sim$1 ms, which is too short to register on most (if not all) data collectors in rheometers. FLOW3D gives the option of either an

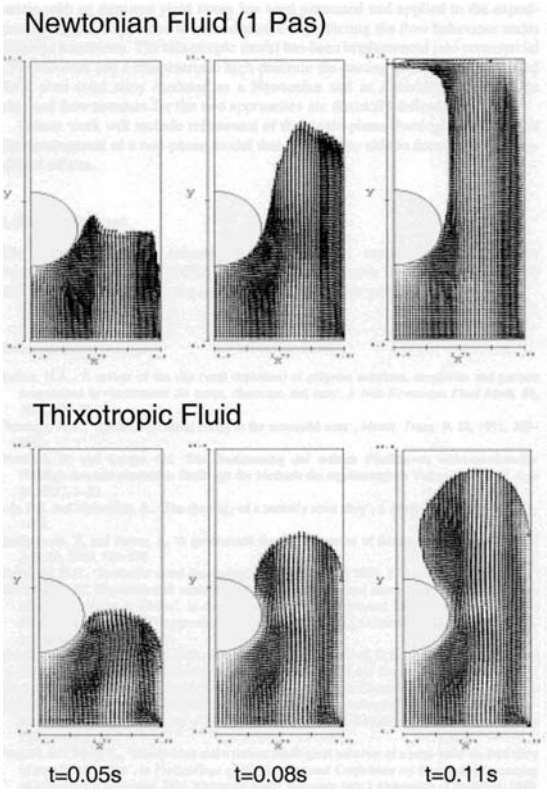

Fig. 7.6 Comparison between simulation of flow into a cavity with a round obstacle assuming Newtonian behavior and assuming thixotropic behavior [73]. The direction of flow is upwards

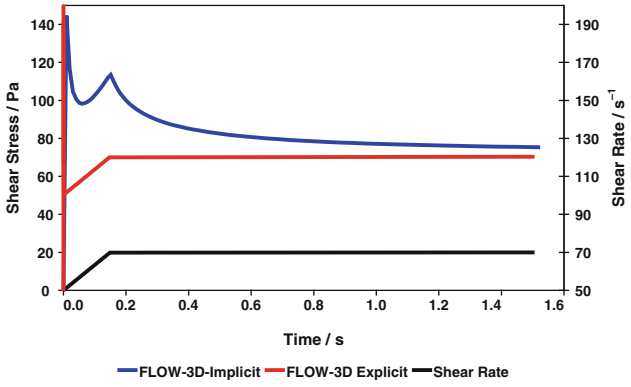

Fig. 7.7 Models of shear rate jump from 50 to 70 s^{-1} in a 1 Pa.s Newtonian fluid in a rotational viscometer [75]. The implicit solver overestimates the width of the momentum diffusion peak

implicit solution or an explicit solution to the Navier–Stokes equation. The shear stress peak height has been modeled with both implicit and explicit solvers [75]. Figure 7.7 shows the result for a linear jump in shear rate from 50 to 70 s^{-1} (with the jump taking 150 ms) in a viscometer. The fluid is Newtonian with a viscosity

of 1 Pa.s. The implicit solver overestimates the length of the momentum diffusion peak, which should last only 1 ms, and its height. The explicit solver accurately reproduces Newtonian behavior, with a very sharp initial momentum diffusion peak. Experiments with a 1 Pa.s Newtonian silicone oil confirmed the explicit prediction.

Only by studying a Newtonian fluid, it was possible to see the overestimation of the momentum diffusion time and the stress produced by the implicit solver. For a shear rate jump in tin–lead (the standard model thixotropic alloy), the solver would be unable to reproduce the acceleration part because the results would combine effects due to thixotropic breakdown with the (overestimated) momentum term. The overestimation will have a small effect on die filling flow patterns, but may not be accurate for predicting the pressure distribution in the die. However, the problem with the explicit solver is that, at high thixoforming viscosities, the computing times are inordinately long. Ward et al. [76] showed that there was a need for a new solver in FLOW3D to cope with the fact that viscosities change over many orders of magnitude in short distances and times. A new alternating direction implicit (ADI) solver was then incorporated. Figure 7.8 shows a comparison of the modeling for a shear rate jump in a viscometer with experimental results (three repeats of the same experiment) and a one-dimensional spread sheet calculation. The fit is reasonable. The potential problems with implicit solvers are not mentioned elsewhere in the literature and it is not clear whether other researchers have tested their modeling for such artifacts.

Thixoforging (as opposed to thixoforming or thixocasting) involves inserting the semisolid (with a relatively high solid fraction) directly between open dies and then bringing the parts of the die together with a ram. Messmer [77] has used FLOW3D to simulate this process, which involves simulating moving die halves. The apparent

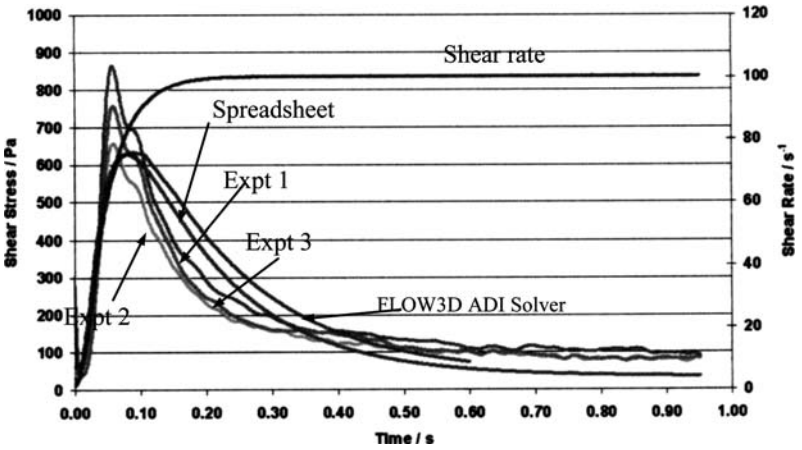

Fig. 7.8 Shear rate jump from 1 to 100 s^{-1} in SnPb alloy ($f_s = 0.36$) showing repeats of the same experiment and modeled fits using a spreadsheet and FLOW-3D predictions with a new ADI solver, which was introduced to address the challenges posed by fluids where the viscosity and shear rate change by many orders of magnitude in short times and spaces [76]

viscosity depends on fraction solid f_s (calculated using the Scheil equation), shear rate $\dot{\gamma}$, and time t The approach is essentially based on that of Barkhudarov et al. [71] with two key equations, one for the equilibrium viscosity η_e and other for the time dependent thixotropic effects:

$$\eta_e = A \exp(Bf_s)\, \dot{\gamma}^m, \tag{7.10}$$

$$\frac{d\eta}{dt} = \beta\,(\eta_e - \eta)\,. \tag{7.11}$$

The viscosity parameters were obtained by fitting the simulation to experimental results with A356 aluminum alloy. The forming force measured at the end of the stroke corresponds well with the simulated force. The early part of the stroke is not well simulated. This is thought to be associated with the use of only one thinning rate, when in practice there may be a series of thinning rates depending on the shear rate. The initial thinning rate is thought to be much higher than that in the final stages. This is consistent with thinking by Ward et al. [76] and with the proposal by Quaak [3] (see Sect. 2.1.1) that at least two different relaxation processes are operating, with different characteristic relaxation times.

FLOW3D has recently been used to analyze the behavior in a drop forge viscometer [30–32] (see section "Parallel Plate Compression"), where a small billet is compressed by a falling steel plate and the compression followed in real time with a video camera [78]. The analysis depends on a numerical model for the coupled motion of a rigid body (the steel plate) and a fluid. It is analogous to that for a plunger, which is pushing a fluid into a die and where the plunger motion is affected by the build-up of pressure in the fluid as it flows into the die.

Kirkwood and Ward [52] use FLOW3D to simulate rapid compression tests between parallel plates. They use a rate equation for the thixotropic breakdown,

$$\tau = \frac{1}{(a + b\dot{\gamma}^m)}, \tag{7.12}$$

where τ is the characteristic time for rapid breakdown or build up to a pseudosteady state structure (not in this case shear stress), and a, b, and m are constants. Experimental results with Al–Si alloy are well represented (Fig. 7.9).

As the soaking time prior to compression is increased, the structure breaks down to a significant extent so that, in low shear rate regions, the flow is close to Newtonian. At shear rates above $100\,s^{-1}$, the rate of breakdown increases dramatically, a finding supported by the drop forge viscometer experiments of Yurko and Flemings [30–32].

MAGMASoft commercial software also has a finite difference thixotropic module, which has been used by a number of researchers. Kim and Kang [79] and Seo and Kang [80] have carried out simulations for a thixotropic fluid obeying the Ostwald-de-Waele power law (i.e., (7.3) but without the yield stress τ_y) with the exponent n taking various values. There is reasonable agreement between the

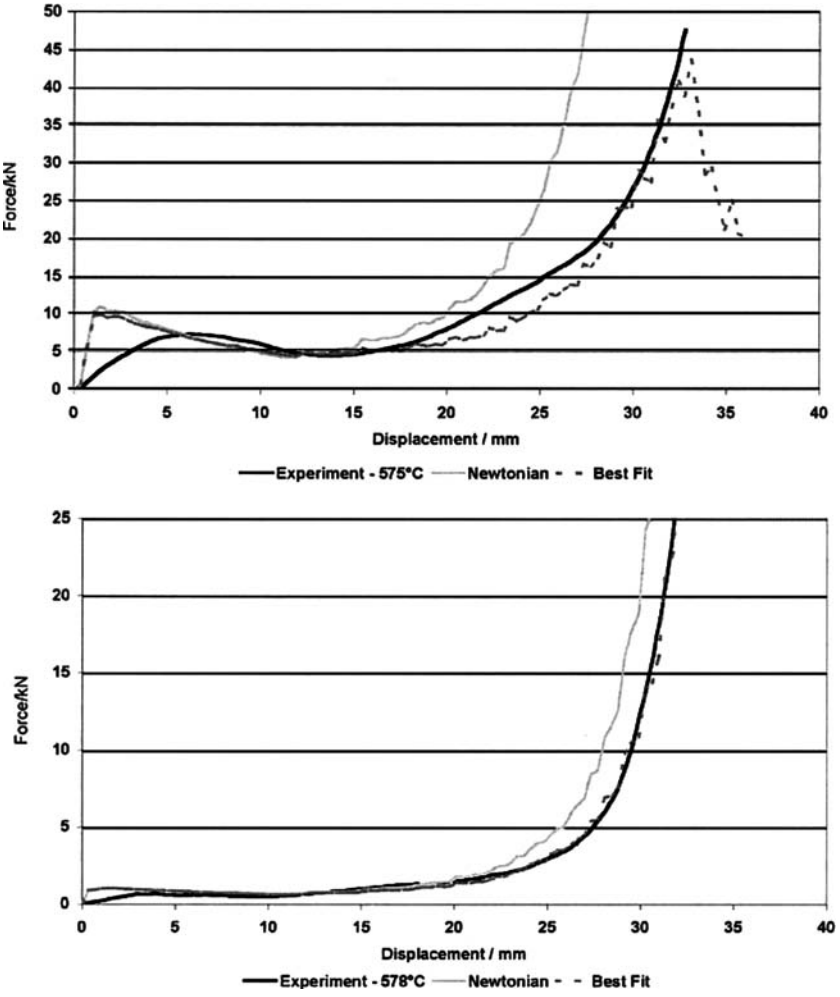

Fig. 7.9 Experimental and modeled results (with FLOW3D) for compression tests on A356 aluminum alloy at two different temperatures [52]. For the higher temperature (578°C), there is hardly any initial peak at the beginning of the curve

simulation and the results of partial filling experiments for components, which do not involve parting of flow fronts and rewelding beyond obstacles or very big changes in section thickness.

Itamura et al. [81] have used a code called Adstefan to compare simulation of die casting, squeeze casting and rheocasting for both metal flow and solidification. Few details are given. The results indicate that there would be fewer shrinkage defects in rheocasting than with the other processes.

7.5.2 Two-phase Finite Difference Modeling

Two-phase finite difference models are rare. In Ilegbusi et al. [68], single phase equations are solved for the whole filling phase. For a given number of particles, the trajectories are computed. It is assumed that the particles will "disappear" when they hit a wall or are trapped in a recirculation zone. Comparing the number of particles at a given distance from the inlet with the total number of injected particles gives a measure of segregation.

7.6 Finite Element Modeling

As for finite difference modeling, both one-phase and two-phase treatments are available. A variety of commercial and other codes are used. The discussion below is grouped according to author(s) for clarity.

7.6.1 One-phase Finite Element Modeling

Zavaliangos and Lawley

Zavaliangos and Lawley [69] use identical equations to Ilegbusi and Brown [67] (based on the model of Brown et al. (see Sect. 3.3)), but without a yield stress. For fractions of solid less than about 0.5, for Sn15%Pb, it is predicted that a free standing billet will collapse. The thixoforming of a simple shape is simulated (in a thixoforging type operation) and the disagglomeration process predicted through the distribution of values of the structural parameter λ (Fig. 7.10). No experimental validation is given in the paper.

Backer

Backer [70] programmed various rheological models into software called WRAFTS. The models included a Newtonian, a shear-thinning model, and an internal variable model, but where, in this case, the variable λ is viewed as a chemical concentration term and its variation with space and time is described by a convective transport equation. The results are shown in Fig. 7.11 for a complex die. With the Newtonian rheological model, the flow front breaks up. There are a number of locations behind cores that remain unfilled as the liquid flows past them. These would then tend to be regions where defects exist in the final component. For the shear thinning model (Fig. 7.11b), the fluid fills behind cores. With the internal variable model, flow tends to occur from the runner at the side of the cavity, rather than that at the bottom. This occurs because the structural parameter λ is reduced as the mixture flows through

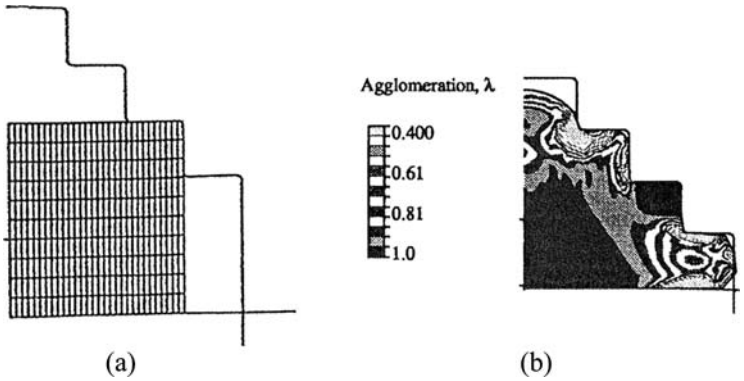

Fig. 7.10 Die filling with semisolid Sn15%Pb ($f_s = 0.55$) [69]. (**a**) Stepped die shape with the undeformed finite element mesh in place ready for deformation. (**b**) Part way through the deformation before die filling is completed showing the distribution of the structural parameter λ, with $\lambda = 1$ representing a structure, which is still fully agglomerated

the runner system from $\lambda = 1$ in the shot sleeve to $\lambda = 0.2$ in the side runner. The value in the bottom runner is 0.4. Thus, the material in the side runner is less viscous and can flow into the cavity more easily. No experimental validation is presented in the paper.

Alexandrou, Burgos and Coworkers

Alexandrou, Burgos and coworkers have published several papers where their approach has gradually been developed [82–88]. They use the commercial code PAMCASTSIMULOR, with a continuous Bingham law based on that introduced by Papanastasiou [89] to avoid the discontinuity in the yield stress. In simple shear terms,

$$\tau = \tau_y \left(1 - \exp\left(-m\dot{\gamma}\right)\right). \tag{7.13}$$

The yield stress τ_y is a function of the fraction solid f_s. When the local stress is higher than τ_y, the slurry behaves as a non-Newtonian fluid with m controlling the exponential rise in the stress at small strain rates $\dot{\gamma}$.

Figure 7.12 shows a comparison of the filling when the fluid is treated as Newtonian and that when it is a Bingham fluid (i.e., the power law exponent n is 1; the fluid is neither shear thinning nor shear thickening, but there is a yield stress). As in Fig. 7.11, the Newtonian fluid tends to jet across the cavity and then flow back on itself, potentially generating defects, particularly behind the core. With the Bingham fluid, the flow fronts meet beyond the core and can merge again. In addition, any oxide films on the surface of the flow front will tend to be incorporated in the component in the Newtonian case, whereas in the Bingham case, the velocity vectors beyond the core are pointing forwards and the oxide will be carried ahead of the flow into overflows, which can be designed in at the end of the flow path.

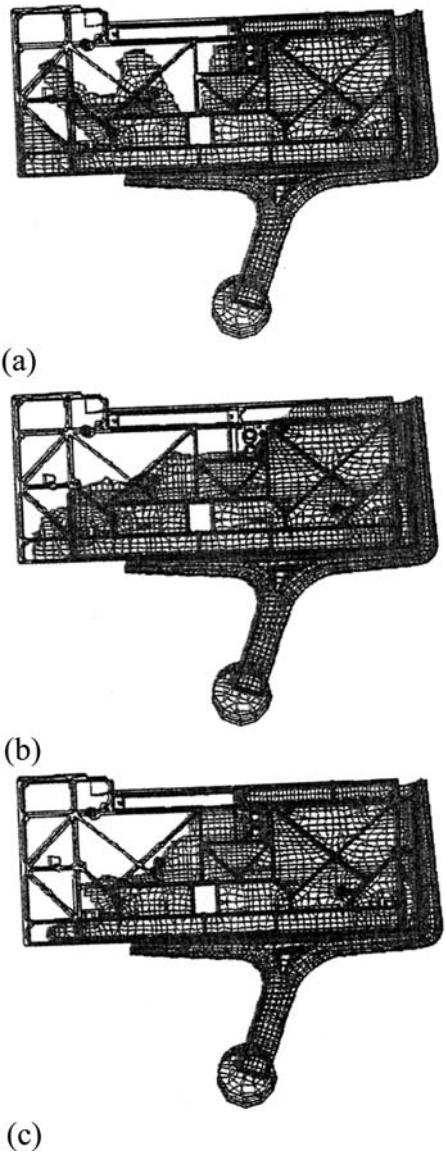

Fig. 7.11 The fluid front for die filling with different viscosity models [70]. (**a**) Newtonian showing break-up of the flow front, (**b**) shear-thinning viscosity with a smoother flow front profile, (**c**) internal variable viscosity again with a smoother profile but with some significant differences from (**b**)

Burgos and Alexandrou [83] simulated a Herschel–Bulkley fluid (i.e., a fluid which obeys a power law dependence of viscosity on shear rate and also has a yield stress) in a sudden three-dimensional square expansion. During the evolution of the flow, two core regions of unyielded material, and dead zones at the corners, are formed.

Pan et al. [84] examine the relative importance of the inertial, viscous, and yield stress effects on the filling profile in a two-dimensional cavity with a Bingham fluid.

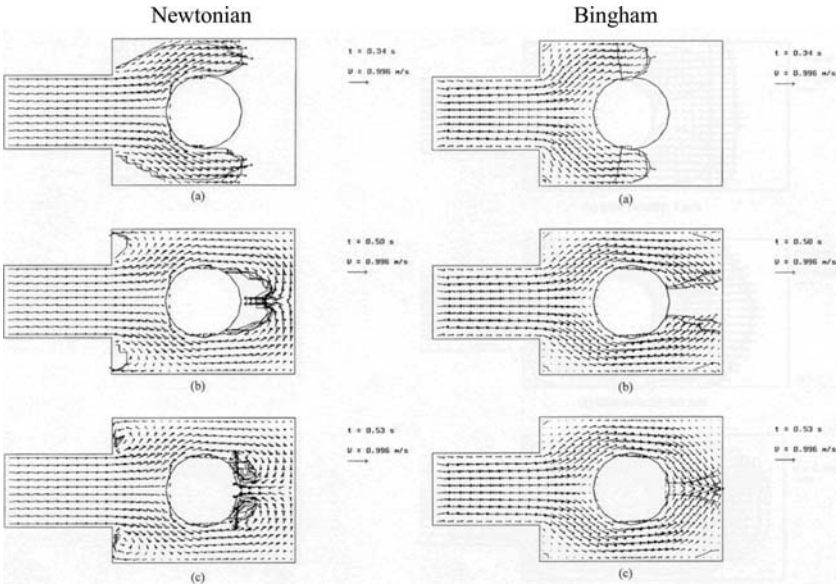

Fig. 7.12 Comparison between Newtonian (*on the left*) and Bingham (*on the right*) filling behavior for a three-dimensional cavity with a cylindrical obstacle [82]

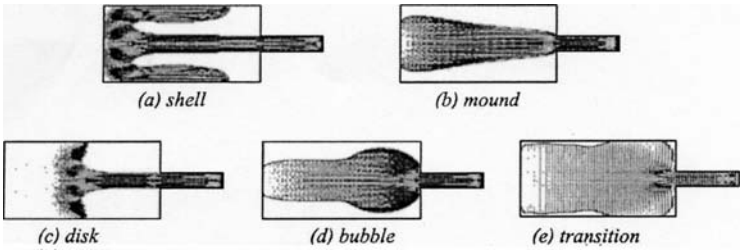

Fig. 7.13 Flow patterns found by modeling for a Bingham fluid in a two-dimensional cavity [84]

Five different flow patterns are identified (Fig. 7.13): "shell" for large Reynolds numbers, but small Bingham numbers; "mound" for low Reynolds and Bingham numbers; "bubble" for larger Bingham numbers; "disk," which occurs between shell and bubble filling and "transition."

The rather powerful approach that emerges here is the capacity to plot maps, such as that in Fig. 7.14, which indicate the regimes where different types of filling are likely to be found. The map plots the Bingham number $\tau_y H/\eta V$ versus the Reynolds number $\rho VH/\eta$ where H and V are characteristic length and velocity scales. The results indicate the importance of the yield stress relative to the inertia forces. Transition flow occupies a narrow region between the disk and the bubble patterns. This region may be prone to instabilities, and hence to defects, as the flow initially starts as a disk and then switches to bubble filling.

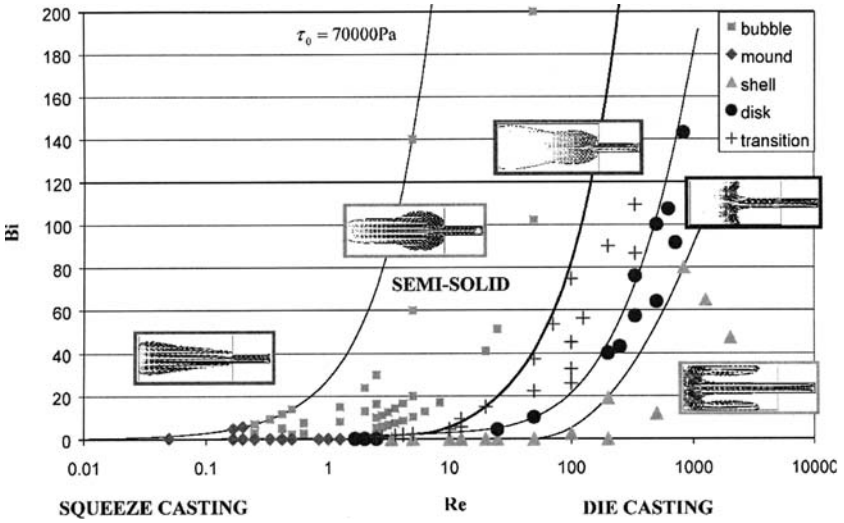

Fig. 7.14 Map showing the flow patterns identified in Fig. 34, plotting Bingham number *Bi* versus Reynolds number *Re* [84]

The approach is expanded by Burgos et al. [85] to include the effect of the evolution of the microstructure via an equation for $d\lambda/dt$, which includes an exponential factor for disagglomeration. This dependence is included to account for the fact that experimentally the shear stress evolution for shear rate step-up experiments is faster than that for the step-down case [3, 11, 23] (see section "Influence of Shear Rate"). Burgos et al. obtain material parameters from experimental work on Sn15%Pb. For flow through a straight square channel, they show that disagglomeration is small in the corners and in the core region of the channel. One of the difficulties is obtaining experimental evidence to back up these predictions of the degree of disagglomeration. One would have to assume that agglomeration can be diagnosed from the number and width of "bridges" between solid globules. However, there are stereological difficulties in identifying whether globules, which are not joined in a two-dimensional section, may be joined in three dimensions [90]. In addition, it would have to be assumed that during a quench no further bonds formed and it is already known that significantly more solid can be laid down on solid globules that exist at the semisolid temperature during a quench at a typical rate [91] (see also Sect. 6.2.3).

Alexandrou et al. [86] and Florides et al. [87] analyzed the flow and shape evolution during the compression of a finite amount of a Bingham plastic under both constant load and constant velocity. Results for various Reynolds and Bingham numbers are presented. There is unyielded material at the top and the bottom of the compressed cylinder, in stagnant layers. These results relate to the compression tests that can be used to obtain rheology parameters for thixotropic materials (see section "Parallel Plate Compression"). However, these particular simulations do not take account of the evolution of the internal structure, i.e., the time and shear rate dependence of the viscosity. There is no detailed comparison with experimental results.

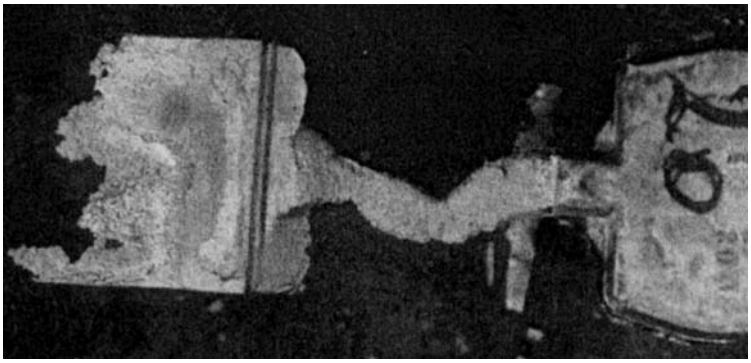

Fig. 7.15 Flow instability of the "toothpaste" type in semisolid processing. The metal is filling from the right to the left [88]

Building on the identification of flow regimes prone to instabilities in [84], Alexandrou et al. [88] have analyzed two-dimensional jets of Bingham and Herschel–Bulkley fluids impacting on a vertical surface at a distance from the die entrance. Shell, disk, and mound patterns, and most transition cases, are all stable, but a bubble pattern gives an unstable jet. Instabilities are the result of finite yield stress and the way the yielded and unyielded regions interact. A common defect in semisolid processing is the "toothpaste effect" (Fig. 7.15) and this analysis gives some insight into the reason for this defect.

Alexandrou and Georgiou [92] have recently modeled the early breakdown of semisolid suspensions in the gap of a cylindrical rheometer in order to provide further insight into the short-term material transients, which are most relevant to the injection of semisolid into a die. A Herschel–Bulkley fluid model is used with the yield stress decomposed into two parts. The first relates to the breakdown during the early stages of deformation (the breakdown of the solid skeleton is referred by Kirkwood and Ward in [52]- see Sect. 6.4). The second part survives the shearing for a long time. The first component is assumed to be a linear function of the coherency parameter. The second component is relevant to steady state experiments.

Orgéas and Coworkers

Orgéas et al. [93] have used the power law cut-off (PLCO) model in Procast commercial software. The material is assumed to be a viscous, isotropic, incompressible fluid. In the Orgéas et al. work, there is one cut-off value $\dot{\gamma}_o$ and this is determined by geometry. Shear thinning only occurs if the shear rate $\dot{\gamma}$ exceeds the cut-off value. Essentially, these researchers are assuming that *agglomeration* probably does not take place over the very short injection times characteristic of thixoforming. Therefore, a decrease of the shear rate $\dot{\gamma}$ will not lead to an increase in viscosity η. A sudden increase of the shear rate *will* lead to a decrease in viscosity. In

effect, an increase in $\dot{\gamma}$ beyond the largest shear rate $\dot{\gamma}_o$ experienced so far will lead to a decrease in viscosity (and modify the maximum shear rate $\dot{\gamma}_o$). It is this "ratchet-type" behavior, which Orgéas et al. model but they assume a single value of $\dot{\gamma}_o$ because they have a simple geometry involving a transition between a shot sleeve and a small injection aperture. Most of the change in viscosity occurs at that point.

Orgéas et al. obtain the parameters for their model from measuring the pressures and the temperatures in a tube with a shaft in it. The simulation then involves the filling of a reservoir. Figure 7.16 shows comparisons between simulations and interrupted filling experiments for A356 alloy.

Orgéas et al. [93] found eutectic-rich concentric rings in the tube in a Poiseuille type experiment (Fig. 7.17). These were due to veins of liquid formed in the shot sleeve as a result of mechanical instabilities in the solid skeleton, which is not

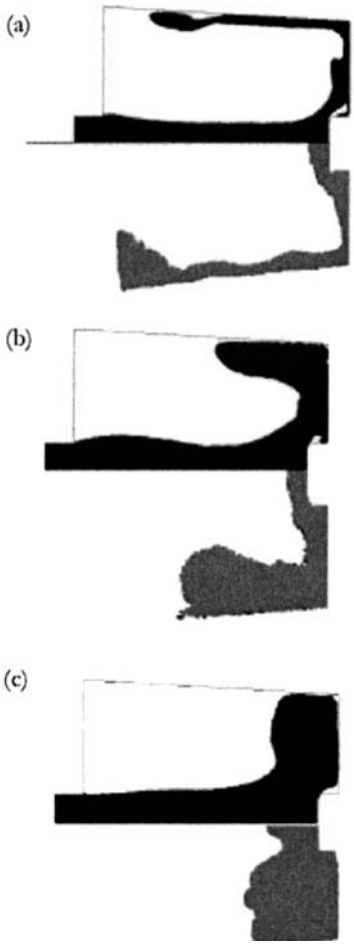

Fig. 7.16 Comparison between experimental and simulated filling of a cavity (initial ram velocity 0.8 ms^{-1}, diameter of tube 25 mm) [93]. (**a**) Fraction solid 0.52. (**b**) Fraction solid 0.58. (**c**) Fraction solid 0.73. In each figure, the *upper part* is the simulation and the *lower part* the experimental result obtained with interrupted filling. The material is flowing into the cavity from the left

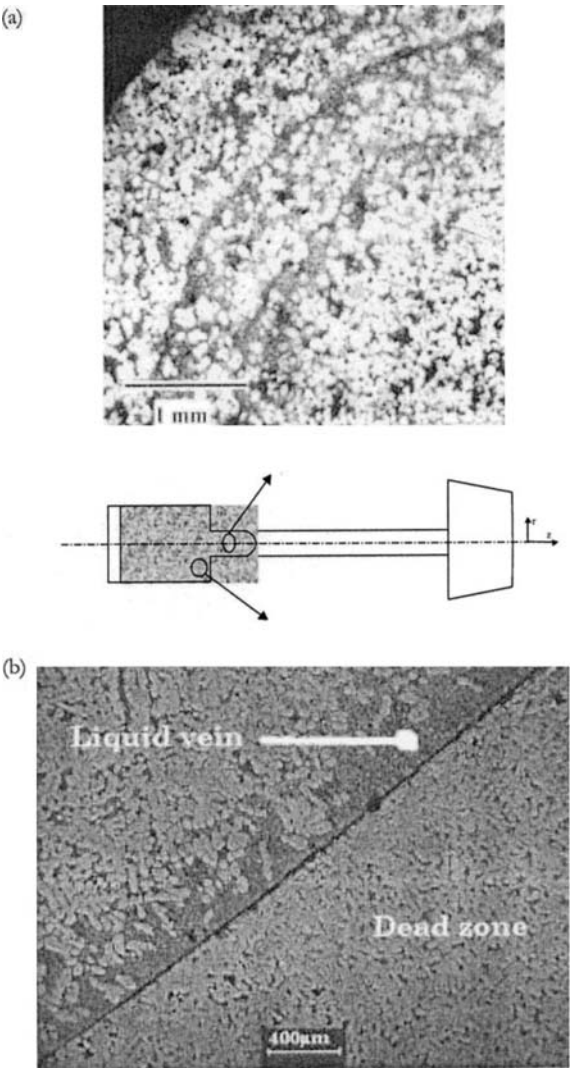

Fig. 7.17 (**a**) Cross-section through the semisolid material solidified in a tube in a Poiseuille-type experiment. The eutectic-rich concentric rings are due to veins of liquid formed in the shot sleeve. (**b**) shows such a vein formed at the limit of the dead zone in the shot sleeve (*see inset*). [93]

uniformly sheared. A "dead zone" formed at the bottom right corner of the shot sleeve, i.e., a zone which hardly suffers any shear and only experiences compression. The compression of the dead zone produces an effect like squeezing a sponge. This type of behavior cannot be predicted with a one-phase model and emphasizes the need for two-phase models, which will be described later. Dead zones need to be avoided in die design for semisolid processing.

Jahajeeah et al. [94] have also used the PLCO model. There is reasonable agreement with the results of interrupted filling tests with A356 aluminum alloy. Defects are predicted with certain runner arrangements and these are found in practice.

7.6.2 Two-phase Finite Element Modeling

Gebelin et al. [95] have presented a useful mathematical comparison of one-phase and two-phase approaches. In addition, there is a detailed introduction by Petera in [96]. Orgéas et al. [93] have also reviewed two-phase approaches.

In the two-phase models, the semisolid material is treated as a saturated two-phase medium, i.e., made of liquid and solid phases. Each phase has its own behavior, which can be influenced by the presence of the other phase via interfacial contributions. The conservation equations can be written within a mixture theory background [97]. The solid phase (which can be thought of as a solid skeleton) can be modeled as a purely viscous and compressive medium [38, 98]. A Darcy-type term appears in the momentum equations to handle the momentum exchanges between the solid and the liquid, which is assumed to be Newtonian [99]. Phase separation (see Fig. 7.11) can be predicted with these models. The principal difficulty, though, is that the determination of the required rheological parameters is not straightforward [38,98]. The computation time also tends to be high because the models require the simultaneous calculation of a solid fraction field, a pressure field, two velocity fields (for the liquid and the solid), and a temperature field (unless the treatment is isothermal).

Zavaliangos [100] uses an internal variable c to represent the degree of cohesion, which evolves with deformation. This is directly analogous with the structural parameter λ in the model of Brown et al. discussed earlier (Sect. 7.3). The behavior is not symmetric under tension and compression (Fig. 7.18). The permeability equation implies that solid–liquid segregation decreases with a reduction in the globule size.

The simulations show that high strain rates result in near undrained conditions and minimal phase segregation. This finding very much reflects the experimental findings, although there are limits. If the strain rate is too high, flow will become turbulent and material will tend to jet across the cavity.

The solid phase is assumed to be a pseudofluid with a Herschel–Bulkley viscosity relationship [101]. The simulation is nonisothermal and has been validated for Sn-15%Pb (Figs. 7.19 and 7.20) with real time visualization of the flow in the die through a transparent window.

Kang and Jung [102] treated the solid phase as compressible and introduced a separation coefficient expressing the actual separation of the particles in relation to their initial separation. As with Zavaliangos [100], the higher the strain rate, the more homogeneous the distribution of the solid fraction. In Binet and Pineau [103], a mixture approach is adopted where the hydrodynamic part is the same as for most incompressible CFD codes, but the velocity field represents the velocities of the mixture. A source term is added to the momentum equations to take account of the diffusion velocities of the different phases. Choi et al. [104] assume the solid to be viscoplastic and use Kuhn's yield criterion for the solid phase (i.e., behavior is symmetric for tension and compression and the hydrostatic component of stress is included). Yoon et al. [105], in contrast, use von Mises yield criterion

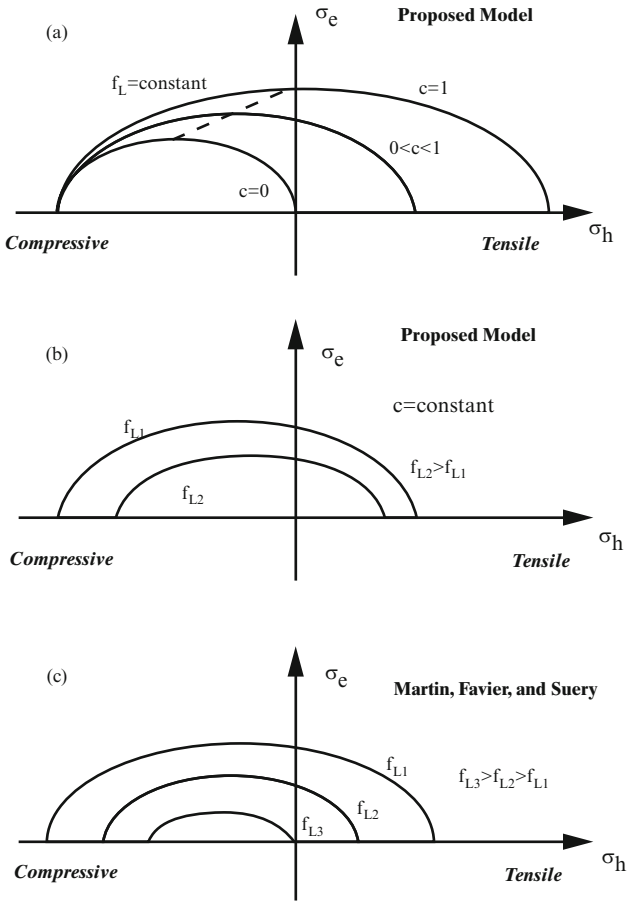

Fig. 7.18 Isopotential curves used in the work by Zavaliangos [100] and compared with that in Martin, Favier and Suery [38]. (**a**) Constant liquid fraction f_L and different levels of cohesion c (c is analogous to the structural variable λ), (**b**) constant cohesion and different f_L, and (**c**) different fractions of liquid f_L [38]. σ_c is the compressive stress and σ_h the hydrostatic pressure in the solid phase

(i.e., symmetric in tension and compression) and treat the semisolid as a single incompressible phase. Kopp and Horst [106] adopt the Drucker–Prager yield criterion (which is asymmetric for tension and compression). Modigell et al. [107] use the pseudofluid approach for the solid phase [108]. All the non-Newtonian properties are shifted to the solid phase and the liquid is Newtonian. Two-dimensional contour maps showing the transitions between laminar, transient, and full turbulent filling are plotted (Fig. 7.21). The three-dimensional process window for A356 aluminum alloy, based on laminar filling is also delineated (Fig. 7.22), providing valuable guidance for actual processing.

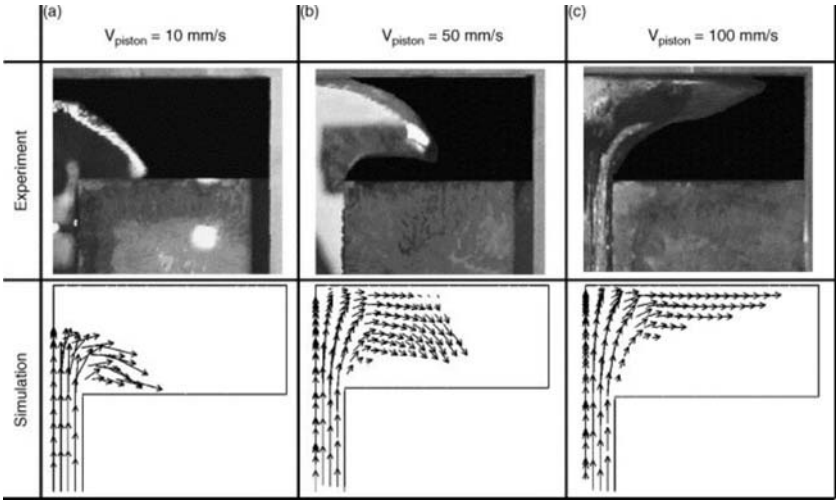

Fig. 7.19 Comparison between the simulated and the observed contours of the flow front for different filling velocities. The simulations have been carried out using one set of model parameters [101]

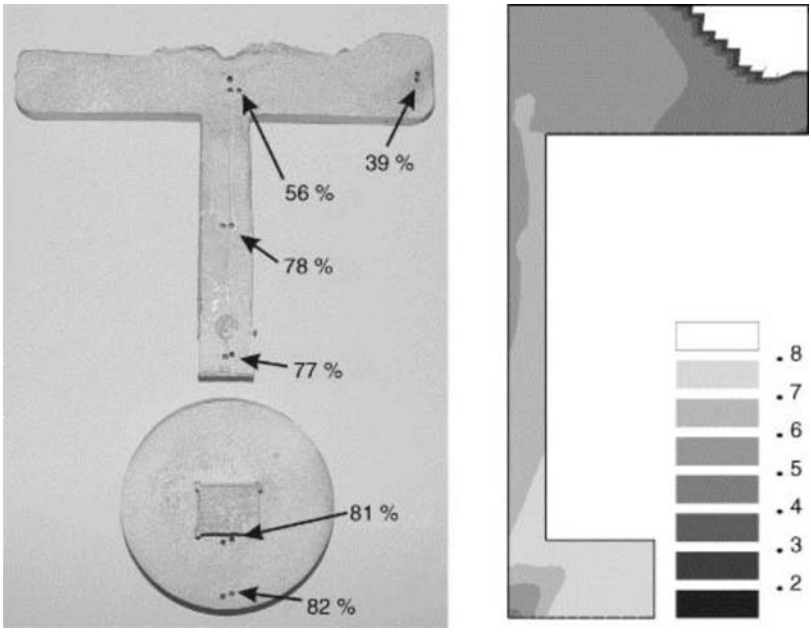

Fig. 7.20 Solid fraction field in the component, based on chemical analysis of the amount of lead (*left*) vs. simulated solid fraction field. Experimental and numerical results for a piston velocity of 50 mm s^{-1} and an initial solid fraction of 62% with Sn15%Pb alloy [101]

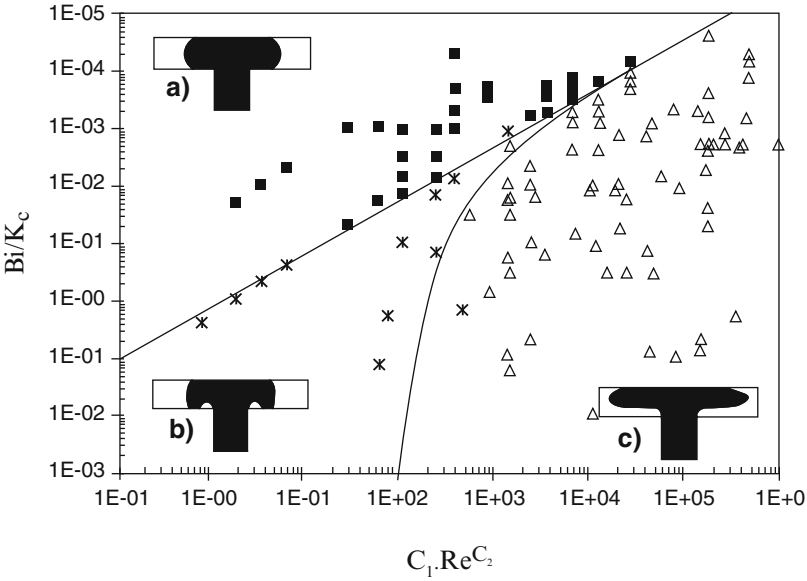

Fig. 7.21 Map of types of flow [107]. (**a**) Laminar, (**b**) Transient, (**c**) Turbulent. *Bi* is the Bingham number, K_c a rheological number, C_1, C_2 geometric constant and *Re* the Reynolds number. K_c, C_1 and C_2 are not specified in the paper

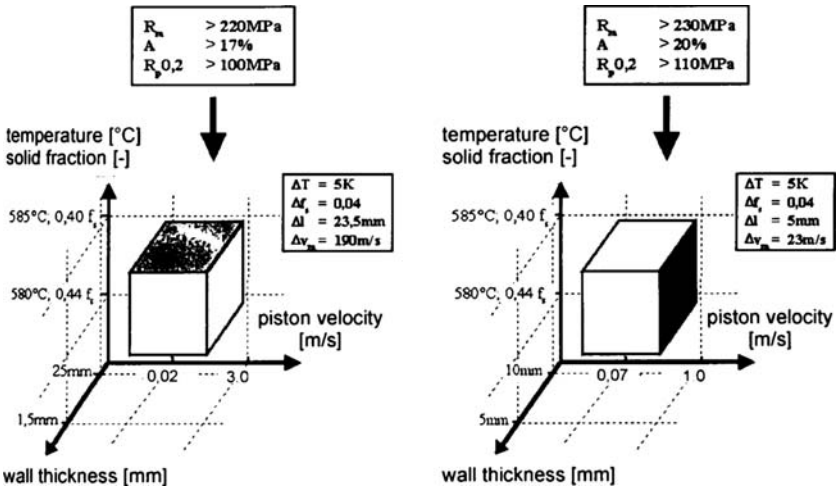

Fig. 7.22 Three-dimensional process window for aluminum alloy A356 [107]. Mechanical properties are given in the *two top boxes*. The *smaller boxes* summarize the process parameter windows to obtain those mechanical properties (ΔT is the temperature window, Δf_s the solid fraction window, Δl the wall thickness and Δv_m). The higher the required mechanical properties, the smaller the three-dimensional process window (compare the *right hand diagram* with the *left*)

7.7 Models akin to Forging Models

7.7.1 Viscoplastic Constitutive Models

Ding et al. [109] used DEFORM-3D software to simulate a rigid viscoplastic alloy being compressed within a six-fingered die heated to the initial temperature of the billet, i.e., the conditions are quasi-isothermal. The researchers fitted the flow stress in the steady state when obtaining the parameters and did not attempt to fit the flow stress during the initial breakdown stage. The die fingers are of different cross-sectional areas. Metal in the larger orifice fingers flows faster than that in the smaller ones. This is contrary to what would be expected with a thixotropic fluid. The simulation is therefore similar to a soft forging simulation. It does, however, include some time dependence in the constitutive equation through a $\dot{\gamma}$ term.

There has been extensive modeling of forging in the solid state and codes, such as FORGE 3 are relatively well established. Some workers (e.g., Rassili et al. [110]) have used viscoplastic constitutive models within such codes to model semisolid forming (Fig. 7.23). The viscoplastic equation is:

$$K\left(\bar{\varepsilon}, T\right) = K_{\mathrm{o}} \exp\left(\frac{\beta}{T}\right) \bar{\varepsilon}^{n}. \tag{7.16}$$

There is no time dependence for the viscosity within these models and these are essentially forging simulations, albeit soft forging. For semisolid processing, where the fraction solid is high (perhaps 80% or more), this may be a valid approach. The process is then a rather different one from where more liquid is present, because the shear thinning behavior of a thixotropic fluid is not occurring and it is rather the softness of material at temperatures just above the solidus, which is being exploited for shape forming.

7.7.2 Model Based on Viscoelasticity and Thixotropy

Thixotropic materials do not normally display viscoelasticity. However, Wahlen [111] presents a model based on viscoelasticity and thixotropy. The inclusion of viscoelasticity suggests that the solid fraction must be rather high and therefore, this model is classified here with those models akin to forging models. There is good agreement between the model and experiment for flow stress versus strain at a temperature of 570°C for A356 aluminum alloy. However, this temperature is such that the alloy would be expected to be nearly fully solid. There is a transition in behavior around 570°C, which the author interprets as the transition between plastic deformation of a connected-particle network and the viscous flow of a suspension of solid particles.

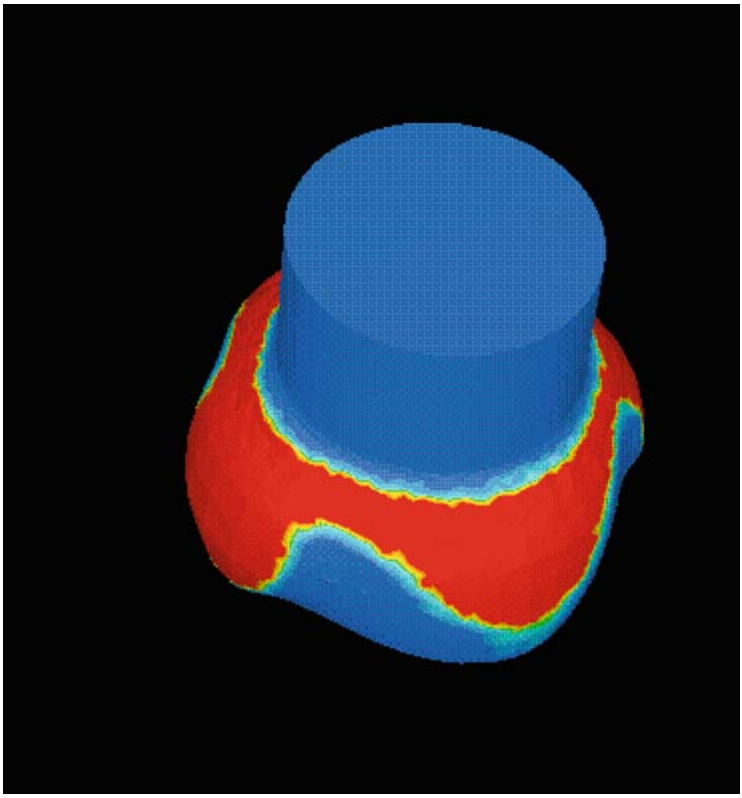

Fig. 7.23 Finite element simulation with FORGE 3 of steel in the semisolid state. The *colors* represent the extent of deformation with *red* high and *blue* low. (Courtesy A. Rassili and coworkers [110])

7.8 Micromodeling

Micromodeling is a novel and interesting approach, which draws on micromechanics and homogenization technique for disordered materials [112]. It is summarized in detail by Favier [113]. It is sometimes referred to as "micro–macro" modeling.

Spherical inclusions (i.e., particles or globules) containing entrapped liquid are assumed to deform very little. They can slip relative to each other if the restriction between them is released. Generally, deformation takes place in the "active zone" around the inclusions, which consists of the solid bonds and that liquid, which is not entrapped. The microstructure is therefore represented as shown in Fig. 7.24, with, in effect, all the inclusions gathered into a single inclusion and this single inclusion coated with the "active zone." The coated inclusion is then embedded into a matrix having the effective properties of the heterogeneous semisolid material (the "homogeneous equivalent medium").

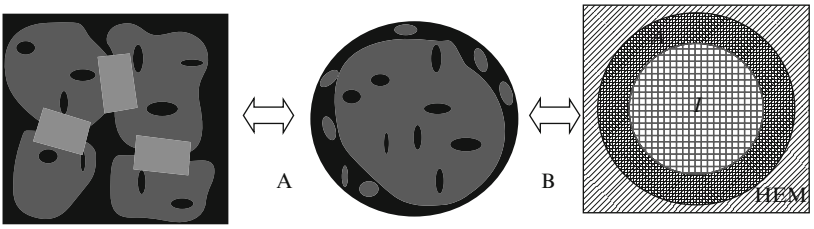

Fig. 7.24 (**a**) shows a schematic representation of the semisolid microstructure showing the presence of one inclusion of solid and entrapped liquid surrounded by a coating of liquid and solid bonds. In (**b**), a coated inclusion is embedded into a matrix having the effective properties of the heterogeneous semisolid material. This is called the "homogeneous equivalent medium" (HEM). [113]

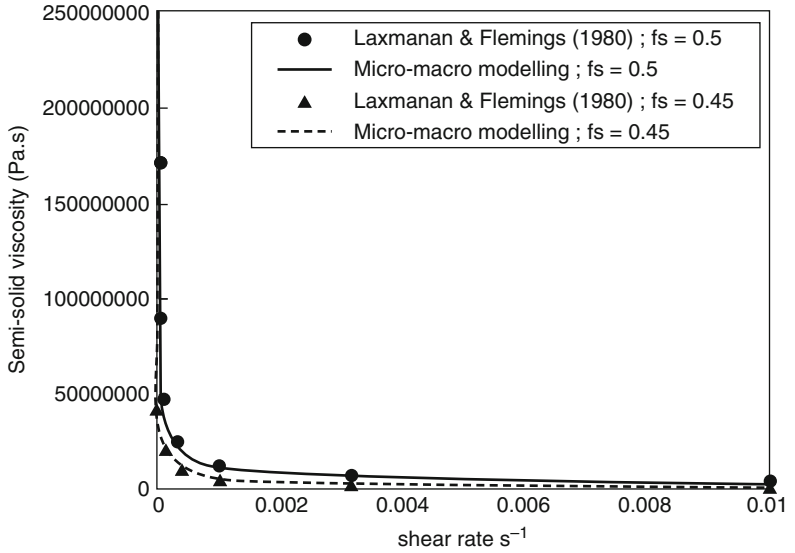

Fig. 7.25 Comparison of "micro–macro" modeling with experimental results for "low" shear rates with Sn15%Pb alloy compressed between parallel plates [45, 113]

The volume solid fraction of the active zone is the internal variable. During deformation, bonds are broken and liquid is released. The liquid–solid distribution therefore changes with strain rate. The liquid and the solid are both assumed isotropic and incompressible. Predictions are compared with experiment in Figs. 7.25 and 7.26. Figure 7.25 is for "low" shear rates and Fig. 7.26 for "high" shear rates, although these are still relatively low in comparison with shear rates in the die in real processing. Note that the parameters for the two fractions of solid in Fig. 7.26 are the same. This is a key test of modeling where often "fitting" of experimental results under one set of conditions is used to obtain the parameters for modeling. To be useful, a model must then be able to accurately predict behavior under a different

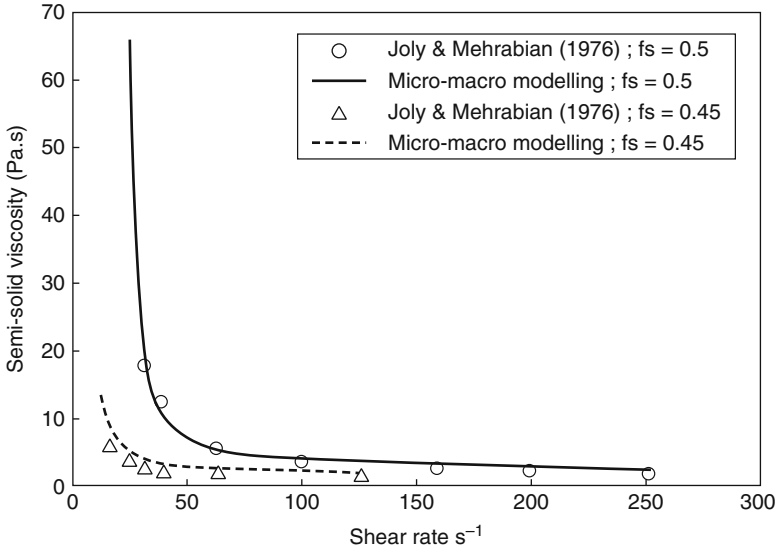

Fig. 7.26 Comparison between "micro–macro" modeling and experimental results for "high" shear rates for Sn15%Pb alloy in concentric cylinder viscometer tests [2, 113]

set of conditions without a "refitting" procedure being necessary. This model is demonstrating this capability.

7.9 Concluding Remarks on Modeling

Modeling of semisolid processing is challenging. It sits on the interface between solid deformation modeling and fluid mechanics, hence placing demands both in mathematical terms, in terms of obtaining the input material parameters and also in terms of sheer computing power. Here, the utility of modeling has been illustrated and issues of whether to use a yield stress in modeling have been highlighted. The use of a structural variable has been described. Models have then been categorized as finite difference or finite element and as one-phase or two-phase. In addition, models which treat semisolid processing as akin to soft forging have been identified. Finally, the approach called "micromodeling" has been outlined.

All modeling must be constantly challenged and validated by experimental results. This can be a matter of comparing with viscometry results (which tend to be for relatively low shear rates) or with compression experiments between parallel plates (where higher shear rates can be achieved). Alternatively, comparison can be made with real die filling. Many workers have carried out interrupted filling tests but inertia tends to continue to carry the material forwards after the stroke has stopped and therefore, the results of interrupted filling must be treated with circumspection. Some real time flow visualization is now available. Where experimental validation is available, this has been identified in this Chapter.